Eur. Phys. J. A **5**, 373–383 (1999)

THE EUROPEAN PHYSICAL JOURNAL A

Dynamic polarization potential of ^{12}C+^{12}C system at molecular-resonance energies

M. Ito[1], Y. Sakuragi[1], Y. Hirabayashi[2]

[1] Department of Physics, Osaka City University, Osaka 558, Japan
[2] Center for Information Processing Education, Hokkaido University, Sapporo 060, Japan

Received: 17 December 1998 / Revised version: 1 March 1999
Communicated by C. Signorini

Abstract. The nuclear reaction dynamics leading to the formation of recently discovered resonance in the mutual-0_2^+ channel of the ^{12}C+^{12}C inelastic scattering around $E_{\rm c.m.} \simeq 32$ MeV is studied in terms of the *dynamic polarization potential* (DPP) induced by the channel coupling among various excited states in ^{12}C. The microscopic 3α cluster-model wave functions are used to generate the ^{12}C–^{12}C diagonal and coupling potentials in the double-folding model. It is found that DPP for the 0_2^++0_2^+ channel is an unusually strong attractive potential which even exceeds the zeroth-order folding-model potential of this channel around the nuclear surface region and that the strong coupling between the 0_2^+ and 2_2^+ states is predominantly responsible for the unusual DPP in this channel. The effective potential, the sum of the original folding-model potential and the attractive DPP, is found to generates resonance states in the same energy region as that of the resonance states generated by the original folding-model potential but the former states are found to be higher-nodal states having four additional radial nodes. Similar but more moderate property of DPP is also found in the entrance (elastic) channel. These results suggest that the reaction dynamics of generating the resonance in the ^{12}C(0_2^+)+^{12}C(0_2^+) channel may rather differ from that of the simple crossing of the zeroth-order molecular band generated by the potentials in the entrance and exit channels suggested by the standard band-crossing model.

PACS. 21.60.Gx Cluster models – 24.10.Eq Coupled-channel and distorted-wave models – 25.70.Ev Resonances – 27.30.+t $20 \leq A \leq 38$

1 Introduction

A broad resonance discovered recently [1,2] in the ^{12}C+^{12}C inelastic scattering at $E_{\rm c.m.} = 32.5$ MeV leading to the ^{12}C(0_2^+)+^{12}C(0_2^+) channel attracted considerable interest. Because the 0_2^+ state of ^{12}C nucleus was known to be a well-developed 3α cluster state [3]–[9], it was initially claimed [1,2] that a *6α linear-chain state* was discovered.[1] The existence of a 6α linear-chain state or similar elongated prolate-shape states in ^{24}Mg were predicted by some theoretical models [10–14] at excitation energies around 15–20 MeV above the 6-α breakup threshold which corresponded to $E_{\rm c.m.}$=30∼35 MeV of the ^{12}C+^{12}C system.

However, more recent experiments [15–21] have raised a serious problem upon the 6α linear-chain interpretation. In the experiments, resonance peaks have been observed also in other exit channels such as ^{12}C(0_2^+)+^{12}C(3_1^-), ^{12}C(3_1^-)+^{12}C(3_1^-) and ^{8}Be$_{\rm gs}$+^{16}O$_{\rm gs}$ channels, which have no affinity with the elongated prolate-shape states. These resonance peaks are well correlated in energy with the resonance observed in the ^{12}C(0_2^+)+^{12}C(0_2^+) channel. Since the elongated prolate-shape states hardly decay through these channels, it would be difficult to identify the 32.5 MeV resonance in the ^{12}C(0_2^+)+^{12}C(0_2^+) channel with the 6α-chain or similar kinds of states.

An alternative interpretation based on the band crossing model [22,23] (BCM) was proposed by Hirabayashi, Sakuragi and Abe [24] to explain the resonance in the ^{12}C(0_2^+)+^{12}C(0_2^+) channel. They performed a coupled-channels (CC) calculation using microscopic form factors based on the microscopic 3α-cluster model [9] for ^{12}C and successfully reproduced the excitation function as well as characteristic angular distributions in this channel [24]. The calculation also reproduced the well-known resonance [25,26] at $E_{\rm c.m.}$=29 MeV in the ^{12}C$_{\rm gs}$+^{12}C(0_2^+) channel. In addition, the same calculation also predicted more resonances in other inelastic channels, such as the ^{12}C(0_2^+)+^{12}C(3_1^-) and ^{12}C(0_2^+) +^{12}C(0_3^+) ones, which have been discovered in a recent experiment [15] by British group at the right position. These results support the validity of the microscopic CC approach to the resonance of these multi-cluster exit channels.

[1] It should be noted that the 0_2^+ state itself is not necessarily the 3α *linear chain* state [7–9].

The results of the CC calculation were interpreted in terms of BCM as the formation of dinuclear resonances having weakly coupled 3α+3α and 3α+$^{12}C_{gs}$ configurations at $E_{c.m.}$=32.5 MeV and 29 MeV, respectively. Namely, the resonances are expected to appear around the energies where the elastic ($^{12}C_{gs}$+$^{12}C_{gs}$) molecular band crosses with the excited bands with the above configurations. In the original BCM, the appearance of prominent resonances is explained solely based on crossing of the molecular rotational bands due to the *intrinsic spins* of excited nuclei, whose stretched coupling to the orbital angular momentum gives rise to an effective increase of moment of inertia of the molecular band [22]. One might think that no such crossing mechanism applies to cases of excitations with intrinsic spin zero, as in the present case of the $^{12}C(0^+_2)$ state. This is true if the moment of inertia of the excited molecular band is the same as that of the elastic one. However, we know that the 0^+_2 state is of a spatially extended 3α structure and, therefore, the interactions between ^{12}C nuclei with one or both in the 0^+_2 state are of longer range than that between the ground state nuclei [27,24]. Thus, the moment of inertia of the excited molecular bands are expected to be larger than that of the elastic one. This makes it possible that the molecular bands in the $^{12}C_{gs}$+$^{12}C(0^+_2)$ and $^{12}C(0^+_2)$+$^{12}C(0^+_2)$ channels cross with the elastic band, as in the cases with normal nonzero-spin channels [27,24].

The resonance energies obtained in the practical CC calculations by Hirabayashi *et al.* [24] are lower by about 5 MeV than the crossing energies of the molecular bands generated by the folding potential in each channel and it was attributed to the channel-coupling effects among various channels included in the CC calculation. We know that the coupling among the three channels, $^{12}C_{gs}$+$^{12}C_{gs}$, $^{12}C_{gs}$+$^{12}C(0^+_2)$ and $^{12}C(0^+_2)$+$^{12}C(0^+_2)$, are rather weak reflecting the large difference of the intrisic nuclear structure between the ground state and the 0^+_2 state and it might be reasonable to attribute the 5 MeV shift of the resonance energies to the coupling effects. However, the CC calculation also included the coupling to other excited states, such as the 2^+_1, 3^-_1 and 2^+_2 states. Since the 2^+_1 and 2^+_2 states are known to have similar nuclear structure to those of the ground state and the 0^+_2 state, respectively, the rather strong coupling to these states can also affect the resonance energies through the *dynamic polarization* effects on the potentials in the entrance channel, $^{12}C_{gs}$+$^{12}C_{gs}$, and the exit ones, $^{12}C_{gs}$+$^{12}C(0^+_2)$ and $^{12}C(0^+_2)$+$^{12}C(0^+_2)$, in which the resonances are observed. The questions to be asked here are how large the channel-coupling effects are and how they affect the inter-nucleus potentials in the entrance and exit channels of interest here. In this paper, we analyze the channel-coupling effects in terms of the so-called *dynamic polarization potentials* [28] (DPP) and investigate the nature of the resonances generated by the CC calculation in connection with the relevant reaction mechanism of this system.

In the next section, we describe the microscopic coupled-channels formalism. In Sect. 3, we calculate DPP of the elastic channel and the $^{12}C(0^+_2)$+$^{12}C(0^+_2)$ one for grazing partial waves and discuss the nature of the resonance wave functions generated by the effective potential with the channel-coupling effect included, namely the sum of the original folding potential and DPP. We also discuss the possible appearance of the effective rotational bands of higher-nodal nature due to the effect of channel coupling. The last section will be devoted to summary and discussion.

2 Microscopic coupled-channel formalism

The theoretical framework and the model space adopted in the present analysis are the same as those used in the previous work [24] but we describe them in more detail in order to define the dynamic-polarization potential (DPP) and to discuss the nature of the coupling potentials explicitly.

The real part of the diagonal and coupling potentials for the ^{12}C+^{12}C system is calculated by the double-folding model [29,33], which is expressed symbolically as

$$V_{ik,jl}(\boldsymbol{R}) = \int \rho_{ij}(\boldsymbol{r}_1)\rho_{kl}(\boldsymbol{r}_2) \times v_{\rm NN}(E,\rho;\boldsymbol{r}_1+\boldsymbol{R}-\boldsymbol{r}_2)d\boldsymbol{r}_1 d\boldsymbol{r}_2. \quad (2.1)$$

A more explicit form of the potentials including the angular-momentum algebra will be given below. In the above equation, $\rho_{ij}(\boldsymbol{r})$ represents the diagonal (i=j) or transition ($i \neq j$) density of ^{12}C. In the present CC calculations, we include the ground state (0^+_1) and the five excited states; the 2^+_1, 0^+_2, 3^+_1 states at excitation energies of 4.44 MeV, 7.65 MeV, 9.64 MeV, respectively and the 2^+_2 and 0^+_3 states. The latter two states have not clearly been identified experimentally, while they are well established theoretically to be well-developed 3α cluster states having similar nuclear structures as that of the famous 0^+_2 state. We have assigned the excitation energies of 10.3 MeV and 14.04 MeV to the 2^+_2 and 0^+_3 states, respectively; the former is the energy of the spin-unknown broad resonance while the latter is a theoretical value taken from [9]. All the diagonal and transition densities among these six states were given by the resonating-group-method (RGM) calculation [9] by Kamimura based on the 3α-cluster model. These densities well reproduce available experimental data for electromagnetic properties of ^{12}C.

In (2.1), $v_{\rm NN}$ represents the nucleon-nucleon (NN) interaction which acts between nucleons belonging to the different nuclei. We adopt the DDM3Y (density-dependent Michigan 3-range Yukawa) interaction [30,31] defined by

$$v_{\rm NN}(E,\rho;\boldsymbol{s}) = g(E,\boldsymbol{s})f(E,\rho),$$
$$f(E,\rho) = C(E)\big[1+\alpha(E)\mathrm{e}^{-\beta(E)\rho}\big]. \quad (2.2)$$

Here, $g(E,\boldsymbol{s})$ is the spin and isospin scalar (S=T=0) component of the original M3Y interaction [32]. It contains a weakly energy-dependent knock-on exchange term having a zero-range form factor [29]. The density dependence of

$v_{\rm NN}$ is represented by the factor $f(E,\rho)$ and the parameter values of $C(E)$, $\alpha(E)$ and $\beta(E)$ are given in [30] as functions of the energy per nucleon E. In the present analysis, we adopt the values evaluated at E=5 MeV, which corresponds to $E_{\rm c.m.}$=30 MeV for the ^{12}C+^{12}C system, and ignore the weak energy dependence over the energy range of interest here. Following the prescription of [30], the density ρ in (2.2) is evaluated by the sum of the densities of the colliding nuclei as $\rho=\rho_1(\boldsymbol{r}_1)+\rho_2(\boldsymbol{r}_2)$, where $\rho_1(\boldsymbol{r}_1)$ ($\rho_2(\boldsymbol{r}_2)$) represents the nucleon density of nucleus 1 (nucleus 2) at the position $\boldsymbol{r}_1$ ($\boldsymbol{r}_2$) with respect to the c.m. of the nucleus. The inclusion of the density dependence is very important, especially for describing large difference of interactions between ^{12}C nuclei in various states having very different nuclear structure; for example the large difference between the interaction for the ^{12}C nuclei both in the spatially compact ground state and that for the ^{12}C nuclei both in the spatially extended 0^+_2 state. In the case of the coupling potential $V_{ik,jl}$ ($i\neq j$ and/or $k\neq l$) defined in (2.1), the nucleons feel different density-environments before and after the transition between different states and, hence, we replace the above $\rho_1(\boldsymbol{r}_1)$ and $\rho_2(\boldsymbol{r}_2)$ with the average densities $\frac{1}{2}\{\rho_{ii}(\boldsymbol{r}_1)+\rho_{jj}(\boldsymbol{r}_1)\}$ and $\frac{1}{2}\{\rho_{kk}(\boldsymbol{r}_2)+\rho_{ll}(\boldsymbol{r}_2)\}$, respectively.

The coupling potential for the Coulomb excitation is also given by the folding model by replacing the nuclear interaction $v_{\rm NN}$ with the Coulomb one in (2.1). However, we have found that the inclusion of the Coulomb coupling is not essential in the discussion about DPP, we neglect the Coulomb coupling in the present paper to save the computational time.

In practical CC calculations, the coupled-channels equations for each total angular momentum of the system, J,

$$\Big[-\frac{\hbar^2}{2\mu}\frac{d^2}{dR^2}+\frac{\hbar^2L(L+1)}{2\mu R^2}+\tilde{V}^{(J)}_{\alpha L,\alpha L}(R)-E_\alpha\Big]\chi^{(J)}_{\alpha L}(R) = -\sum_{(\beta,L')\neq(\alpha,L)}V^{(J)}_{\alpha L,\beta L'}(R)\chi^{(J)}_{\beta L'}(R) \tag{2.3}$$

are solved numerically. Here, α or β denotes the "channel" designated by the intrinsic spins of the two ^{12}C nuclei, I_1 and I_2, the channel spin I ($\boldsymbol{I}=\boldsymbol{I}_1+\boldsymbol{I}_2$), and the sum of the excitation energies of two ^{12}C nuclei, ε_α. Thus, $E_\alpha\equiv E-\varepsilon_\alpha$ is the energy of the ^{12}C–^{12}C relative motion in the channel α, while $\chi^{(J)}_{\alpha L}(R)$ represents the radial wave function of the relative motion in the "sub-channel" specified by α, J and L (L being the orbital angular momentum). The diagonal or coupling potential, $V^{(J)}_{\alpha L,\beta L'}(R)$, between the sub-channels (α, J, L) and (β, J, L') is given by the double-folding model as mentioned before and its explicit form reads

$$\begin{aligned}V^{(J)}_{\alpha L,\beta L'}(R) &= V^{(J)}_{I_1I_2IL,I_1'I_2'I'L'}(R)\\ &= \big\langle\Phi^{(JM)}_{I_1I_2IL}(\boldsymbol{\xi}_1,\boldsymbol{\xi}_2,\hat{\boldsymbol{R}})\big|\sum_{\substack{i\in C_1\\ j\in C_2}}v_{\rm NN}(\boldsymbol{x}_{ij})\\ &\quad\times\big|\Phi^{(JM)}_{I_1'I_2'I'L'}(\boldsymbol{\xi}_1,\boldsymbol{\xi}_2,\hat{\boldsymbol{R}})\big\rangle_{\boldsymbol{\xi}_1,\boldsymbol{\xi}_2,\hat{\boldsymbol{R}}},\end{aligned} \tag{2.4}$$

where

$$\begin{aligned}&\Phi^{(JM)}_{I_1I_2IL}(\boldsymbol{\xi}_1,\boldsymbol{\xi}_2,\hat{\boldsymbol{R}})\\ &=\sqrt{\frac{1}{2(1+\delta_{I_1I_2}\delta_{i_1i_2})}}\\ &\quad\times\mathcal{S}_{12}\Big[\big[\psi^{(i_1)}_{I_1}(\boldsymbol{\xi}_1)\otimes\psi^{(i_2)}_{I_2}(\boldsymbol{\xi}_2)\big]_I\otimes i^LY_L(\hat{\boldsymbol{R}})\Big]_{JM}\\ &=\sqrt{\frac{1}{2(1+\delta_{I_1I_2}\delta_{i_1i_2})}}\\ &\quad\times\Big\{\Big[\big[\psi^{(i_1)}_{I_1}(\boldsymbol{\xi}_1)\otimes\psi^{(i_2)}_{I_2}(\boldsymbol{\xi}_2)\big]_I\otimes i^LY_L(\hat{\boldsymbol{R}})\Big]_{JM}\\ &\quad+\Big[\big[\psi^{(i_1)}_{I_1}(\boldsymbol{\xi}_2)\otimes\psi^{(i_2)}_{I_2}(\boldsymbol{\xi}_1)\big]_I\otimes(-1)^Li^LY_L(\hat{\boldsymbol{R}})\Big]_{JM}\Big\}\end{aligned} \tag{2.5}$$

is the channel wave function, which is symmetrized [23] with respect to the exchange of identical ^{12}C nuclei by the symmetrization operator $\mathcal{S}_{12}$. Here, $\psi^{(i_1)}_{I_1}$ denotes the internal wave function of ^{12}C in the i_1th state having an intrinsic spin I_1: e.g. i_1=2 and I_1=0^+ for the 0^+_2 state, which is given by the microscopic 3α RGM calcualtion [9] as mentioned before. In (2.4), $v_{NN}(\boldsymbol{x}_{ij})$ represents the NN interaction between the ith nucleon in a nucleus C_1 and the jth one in the other nucleus C_2, for which we adopt the DDM3Y interaction as already mentioned.

The channels included in the present CC calculation are the same as those in [24], namely the elastic (0^+_1+0^+_1) channel, the single-excitation channels in which one of the ^{12}C nuclei is excited to either 2^+_1, 3^-_1, 0^+_2, 2^+_2 or 0^+_3 states, and the mutual-excitation channels in which two ^{12}C nuclei are in the excited states as 2^+_1+2^+_1, 0^+_2+2^+_1, 0^+_2+0^+_2, 0^+_2+3^-_1, 0^+_2+0^+_3, 0^+_2+2^+_2 and 2^+_2+2^+_2. The coupling among all these channels are fully taken into account.

Once we fix the model space (namely the channels), there is no free parameter in the present formalism, except the imaginary potential which we have introduced in the diagonal part of the interactions in order to account for the absorption of flux to fusion and other reaction processes. Namely, we have replaced the diagonal potential $V^{(J)}_{\alpha L,\alpha L}(R)$ defined by (2.4) with

$$\tilde{V}^{(J)}_{\alpha L,\alpha L}(R)\equiv V^{(J)}_{\alpha L,\alpha L}(R)+iW(R) \tag{2.6}$$

in the left-hand side of (2.3). We have used the three-parameter Woods-Saxon form for $W(R)$ and the parameters are taken to be common to all the channels, as in the case of the previous study [24].

In the present study, however, we have slightly modified the parameter values from those of [24]. This is because in the previous analysis there was an approximate treatment in the symmetrization process of (2.5) in the calculation of coupling potentials among some mutual-excited channels, while we calculate them exactly in the present paper. Therefore, we have slightly modified the imaginary-potential parameters so that we obtain the

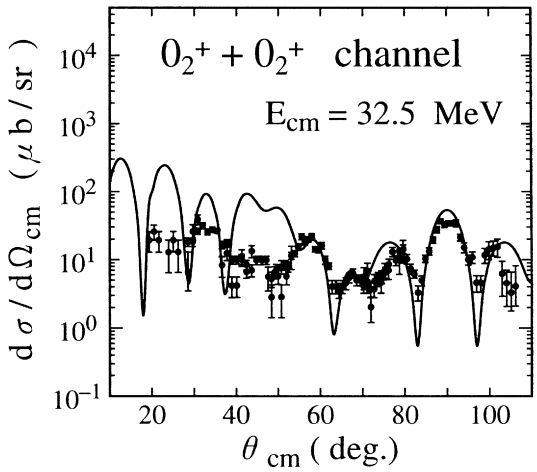

Fig. 1. Differential cross section of the ^{12}C+^{12}C inelastic scattering to the 0_2^++0_2^+ channel at $E_{\rm c.m.}$=32.5 MeV. The solid curve is the result of the CC calculation. The experimental data are taken from 1)

same quality of fits as those obtained in the previous work [24]. In order to demonstrate the quality of fits, we show in Fig. 1 the angular distribution of the ^{12}C(0_2^+)+^{12}C(0_2^+) channel at the on-resonance energy ($E_{\rm c.m.}$=32.5 MeV) as a typical example. The parameter values obtained at this energy are W_0=20.0 MeV, a=0.20 fm and R=3.0 fm. In the comparison with the fit shown in Fig. 3 of [24], one may notice that the present calculation gives about 50% larger cross sections at the forward angles ($\theta < 50°$) and gives rise to an extra bump around $\theta = 50°$ but the difference at those forward angles is not essential for the discussion of resonance phenomena observed in the backward-angle cross sections (θ=70–105°). We have confirmed that the minor modification introduced in the present paper does not affect the essential agreement with a wide range of experimental data attained in [24].

3 Dynamic polarization potential

The dynamic polarization potential (DPP) discussed in the present paper is the so-called *trivially-equivalent local potential* [28] (TELP) or equivalently called, *wave-function-equivalent local potential* [33,34], which is defined as

$$\Delta V^{(J)}_{\alpha L}(R) = \sum_{(\beta,L')\neq(\alpha,L)} V^{(J)}_{\alpha L,\beta L'}(R)\chi^{(J)}_{\beta L'}(R)/\chi^{(J)}_{\alpha L}(R). \quad (3.1)$$

After solving the CC equations, we have numerical values of the wave functions $\chi^{(J)}_{\alpha L}(R)$ and $\chi^{(J)}_{\beta L'}(R)$ of all the channels in hands. Thus, we can directly calculate DPP numerically. By definition, DPP of this type is "exact" in the sense that $\tilde{V}^{(J)}_{\alpha L,\alpha L}(R) + \Delta V^{(J)}_{\alpha L}(R)$ exactly reproduces the coupled-channel solution for this channel, $\chi^{(J)}_{\alpha L}(R)$. Namely, $\chi^{(J)}_{\alpha L}(R)$ satisfies the following "single-channel"

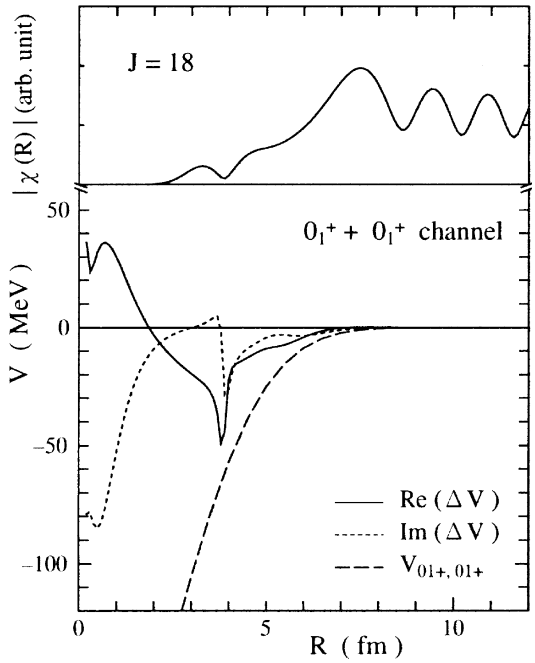

Fig. 2. The real part (solid) and the imaginary part (dotted) of DPP of the elastic channel for J=18 (lower) and the modulus of the elastic-channel wave function (upper). The long-dashed curve shows the folding potential of this channel

Schrödinger equation equivalent to the CC equations defined in (2.3);

$$\Big[-\frac{\hbar^2}{2\mu}\frac{d^2}{dR^2} + \frac{\hbar^2 L(L+1)}{2\mu R^2} + \tilde{V}^{(J)}_{\alpha L,\alpha L}(R) + \Delta V^{(J)}_{\alpha L}(R) - E_\alpha \Big]\chi^{(J)}_{\alpha L}(R) = 0. \quad (3.2)$$

In (3.1), each term of the r.h.s. represents the contribution from individual channels $\{(\beta, J, L')\}$ to DPP of the channel (α, J, L), which may provide useful information for understanding the origin of DPP and the relevant reaction dynamics, as will be discussed below. In the previous study [24], it was found that the most important partial wave around the resonance energy was J=18. Therefore, we first discuss DPP for J=18 in some detail in the resonance energy region.

3.1 DPP for the entrance channel

Figure 2 shows the real and imaginary parts of DPP for J=18 in the entrance (elastic) channel calculated at $E_{\rm c.m.}$=32.5 MeV. For comparison, the diagonal (folding-model) potential of this channel is shown by the long-dashed curve. The modulus of the radial wave function of this channel is also shown in the upper panel of the figure in an arbitrary unit. The irregular cusp-like shapes of DPP around R=4 fm are due to the minimum of the wave fucntion which appears in the denominator in (3.1), while the large values at short distances ($R \leq$2 fm) stem from the almost zero-value of the wave function. The behavior

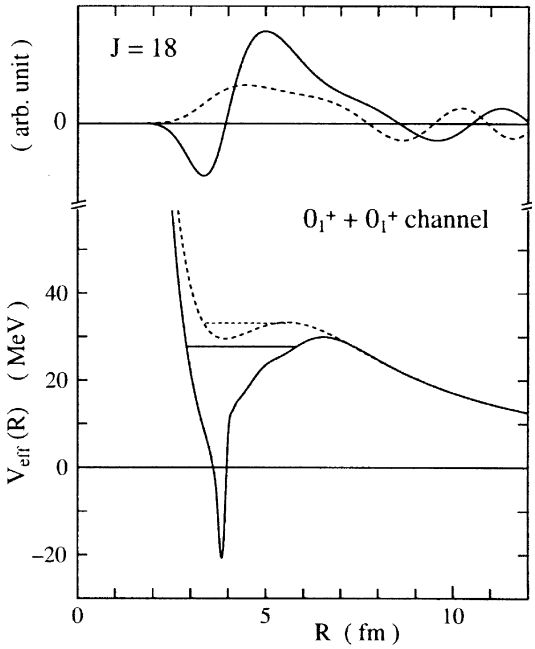

Fig. 3. The effective potentials for $J(=L)=18$ (lower) of the elastic channel and the wave functions of the barrier-top resonances (upper). The solid and dotted curves correspond to the cases with and without the inclusion of DPP, respectively. The holizontal bars indicate the energy positions of the resonances

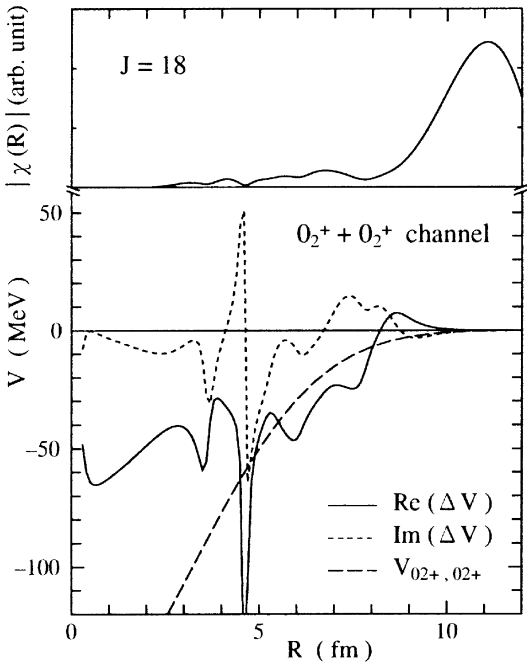

Fig. 4. The same as Fig. 2 but for the $0_2^+ + 0_2^+$ channel

of DPP at such short distances has little effect upon the scattering of high partial waves because of the dominance of the centrifugal potential in this radial region. Therefore, we concentrate our attention to the behavior of DPP around the surface region. It is seen that the real part of DPP is predominantly attractive around the surface region having 30–50 % of the strength of the zeroth-order folding potential. It is noticed that the strength of DPP amounts to about 10 MeV at R=5 fm and 5 MeV at R=6 fm. The imaginary part of DPP also has a considerable strength around the barrier region with negative sign.

In order to see the effect of the channel coupling on the resonance formation and on the nature of the resonance wave function more clearly, we calculate the scattering with the real folding-model potential alone with and without the real part of DPP added. Without DPP, the barrier-top position of the effective potential (the sum of the nuclear, Coulomb and centrifugal potentials) for $J(=L)=18$ is around R=5.5 fm and its barrier height is about 33 MeV, as shown by the dotted curve in the lower half of Fig. 3. This potential gives rise to a barrier-top resonance at $E_{\rm cm}$=32.5 MeV, the wave function of which is shown by the dotted curve in the upper half of Fig. 3. It is seen that the resonance wave function has no radial node inside the barrier region ($R \leq$5.5 fm), to which we could assign a total oscillator quantum number $N \equiv 2n+L=18$, where n is the number of radial nodes. Addition of the real part of DPP to this potential gives rise to a considerable change of the barrier-top position and its height, as shown by the solid curve of the same figure. This modified effective potential generates a barrier top resonance at $E_{\rm cm}$=27.7 MeV, which is 5.4 MeV below the resonance generated by the original potential. The wave function of this resonance, however, has one radial node (n=1) inside the barrier regin ($R \leq$6.5 fm) as shown by the solid curve, which corresponds to a higher-nodal state with $N \equiv 2n + L$=20 compared with the resonance generated by the original potential. This implies that the original resonance with N=18 has been pulled down more deeply by the attraction of DPP, although it is not visible in scattering due to the extremely small width.

It should be noted that DPP itself is energy dependent and, hence, DPP evaluated at 27.7 MeV is not precisely identical to that evaluated at 32.5 MeV. Therefore, the above statement that the DPP evaluated at $E_{\rm cm}$=32.5 MeV gives rise to a resonance at $E_{\rm cm}$=27.7 MeV may not necessarily be consistent. However, we have confirmed that the strongly attractive nature of DPP around and inside the barrier region is common to all the nearby energies, although details of the radial shape are somewhat different depending on energy. Thus, the qualitative discussion that the resonance state of higher-nodal nature is induced by the channel-coupling effect remains valid.

3.2 DPP for the exit channels

Next, we calculate DPP of the $0_2^+ + 0_2^+$ channel. Here, DPP of this channel is calculated from the solutions of the CC equations under the boundary condition that the $0_2^+ + 0_2^+$ channel is the "entrance channel", and the energy for the relative motion E_α in this channel is taken to be the $E_\alpha = E_{\rm c.m.} - \varepsilon_\alpha$ where $E_{\rm c.m.}$=32.5 MeV and ε_α is the Q-value of this channel, namely twice the excitation energy of the 0_2^+ state. The result is shown in Fig. 4. The diagonal (folding-model) potential of this channel is also shown

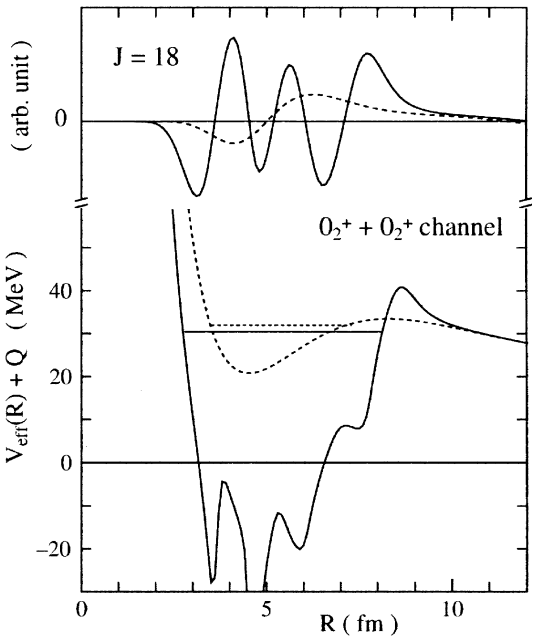

Fig. 5. The same as Fig. 3 but for the $0_2^+ + 0_2^+$ channel. In the ordinate, Q denotes the Q-value of this channel, which is twice the excitation energy of the 0_2^+ state

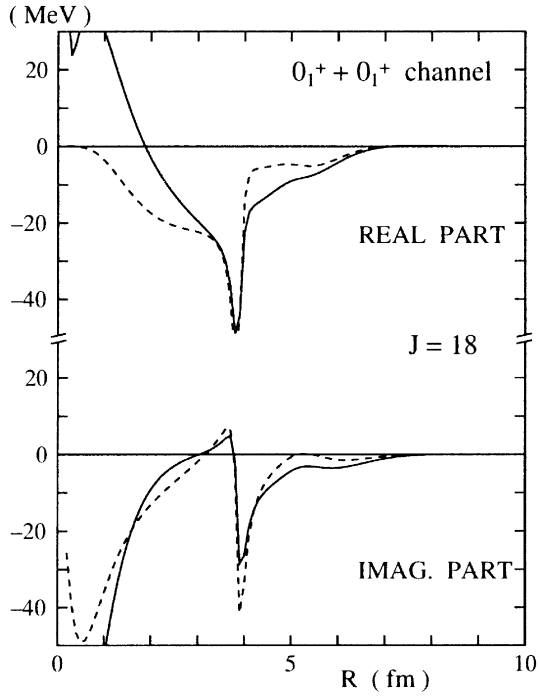

Fig. 6. The real part (upper) and the imaginary part (lower) of DPP of the elastic channel for J=18. The dotted curves show the contribution from the $0_1^+ + 2_1^+$ channel

by the long-dashed curve for comparison. The strength of DPP of this channel is surprisingly large, the real part of which even exceeds the zeroth-order folding potential of this channel at the surface region of interest here, as shown by the solid curve. Again, the irregular behaviors of DPP around R=3.5 fm, 4.7 fm, 6.0 fm and 7.7 fm are due to the minima of the wave function of this channel which is shown in the upper half of the figure. The attractive strength of DPP amounts to 20–30 MeV around the grazing distances ($R \simeq 7 \sim 8$ fm) of this channel. It is, however, interesting to notice that the real part changes its sign from negative to positive around R=8.2 fm, which happened to coincide with the barrier-top position of the effective potential generated by the original folding potential (the dotted curve in the lower half of Fig. 5). Therefore, the addition of DPP to the original effective potential leads to a very strange shape of the barrier shown by the solid curve in Fig. 5.

This modified effetive potential with the real part of DPP generates a resonance state at $E_{\mathrm{c.m.}}$=30.4 MeV, close to the resonance state generated at $E_{\mathrm{c.m.}}$=32.0 MeV by the original effective potential, as shown by the solid and dotted bars in the lower half of Fig. 5. The wave functions of these resonance states are shown by the solid and dotted curves in the upper half of the figure. The wave function generated by the original potential (the dotted curve) has one radial node (n=1) inside the barrier and, hence, corresponds to the member of the molecular rotational band with N=20. Despite the similar resonance energies, the wave function of the new resonance state (the solid curve) has additional four radial nodes (namely, n=5) compared with the wave function of the original resonance, which implies that the new resonance state corresponds to the state with N=28. This is an ineviable consequence of the drastic increase of attraction by adding DPP, namely by the strong channel-coupling effects.

We have also calculated DPP for the $0_1^+ + 0_2^+$ channel and found that its qualitative nature is quite similar to that of the $0_2^+ + 0_2^+$ channel just mentioned above, although we do not show them in figures. Since the essential mechanism to generate such a characteristic property of DPP is common to these exit channels as disucussed below, we focus our attention to the $0_2^+ + 0_2^+$ channel in the rest part of this paper.

3.3 DPP and the coupling scheme

Next, we investigate the roles of the individual channels contributing to DPP discussed above, by looking at the individual terms in the r.h.s. of (3.1) separately, and find out which channels play important roles for DPP of the elastic channel and the $0_2^+ + 0_2^+$ one, respectively. First, we have analyzed DPP of the elastic channel and found that the dominant contribution comes from the $0_1^+ + 2_1^+$ single-excitation channel, as shown by the dashed curves in Fig. 6. It is seen that more than one half of the full strength of DPP stems from the contribution of this channel, while the rest part is found to be shared by the contributions from the $2_1^+ + 2_1^+$, $0_1^+ + 3_1^-$ and $0_1^+ + 0_3^+$ channels, although the $2_1^+ + 2_1^+$ channel is the most important next to the $0_1^+ + 2_1^+$ channel. The contribution from other channels is found to be almost negligible.

For DPP of the $0_2^+ + 0_2^+$ channel, the most important contribution to DPP comes from the $0_2^+ + 2_2^+$ channel,

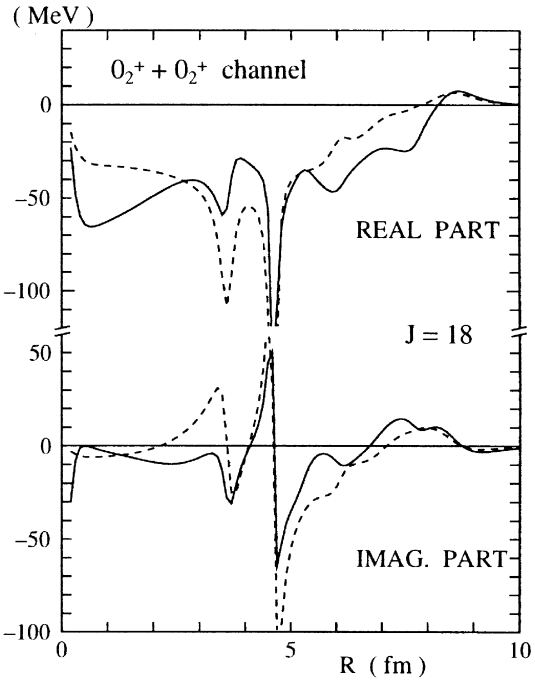

Fig. 7. The real part (upper) and the imaginary part (lower) of DPP of the 0_2^++0_2^+ channel for J=18. The dotted curves show the contribution from the 0_2^++2_2^+ channel

which is shown by the dashed curves in Fig. 7 together with the total DPP (the solid ones). The contribution of this channel carries about 50% of the total strength of DPP around the grazing region and the rest half is attributed to the $[2_2^+ \otimes 2_2^+]_I$ channels with the channel spins I=0, 2 and 4. Among the $[2_2^+ \otimes 2_2^+]_I$ channels, the I=4 channel is found to give the largest contribution. The contributions of all other channels are found to be almost completely negligible and invisible in the present energy scale of Fig. 7.

In order to understand the reason why only some specific channels contribute to DPP of either the elastic channel or the 0_2^++0_2^+ one and, particularly, to understand the extremely large values of DPP of the latter channel, we look into details of the transition densities and the relevant coupling potentials among various channels.

A key to understand the characteristic coupling scheme of the present ^{12}C+^{12}C system is the coexistence of two groups of states having very different nuclear structures, i.e. the *shell-like states* (such as the 0_1^+ and 2_1^+ states) and the *3α-cluster states* (such as the 0_2^+ and 2_2^+ states), as mentioned before. Because of the large difference of nuclear structure, the transitions between the states having different structures are weak, while the transitions among the same group of states are strong. The large difference of nuclear structure gives rise to the difference in shapes and strengths of the transition densities [9] among these states in ^{12}C. In Fig. 8a, we compare the quadrupole (λ=2) transition densities among the 0_1^+, 2_1^+, 0_2^+ and 2_2^+ states, which have been used in the present CC calculation. A large spatial range of the $2_2^+ \rightarrow 0_2^+$ transition density reflects the spatially-extended 3α-cluster structure of these states. The calculated B(E2) value for this transition is about 25 times larger than that for the $2_1^+ \rightarrow 0_1^+$ transition. [9]

The large difference of the transition densities reflects upon the coupling potentials for the corresponding transitions through the folding procedure of (2.1) or equivalently of (2.4). Figure 8b shows the J=L'=L=18 component of the coupling potentials, $V^{(J)}_{I_1 I_2 I L, I_1' I_2' I' L'}(R)$ defined in (2.4), for the transition between the elastic channel $[0_1^+ \otimes 0_1^+]_{I=0}$ and the $[0_1^+ \otimes 2_1^+]_{I=2}$ channel (the dashed curve), that between the $[0_2^+ \otimes 0_2^+]_{I=0}$ channel and the $[0_2^+ \otimes 2_2^+]_{I=2}$ one (the solid curve), that between the $[0_2^+ \otimes 0_2^+]_{I=0}$ channel and the $[0_2^+ \otimes 2_1^+]_{I=2}$ one (the dotted curve), and that between the $[0_1^+ \otimes 0_1^+]_{I=0}$ channel and the $[0_1^+ \otimes 2_2^+]_{I=2}$ one (the dot-dashed curve), each of which contains the corresponding transition density shown in Fig. 8a. The large magnitude of the coupling potential for the transition between the $[0_2^+ \otimes 0_2^+]_{I=0}$ and $[0_2^+ \otimes 2_2^+]_{I=2}$ channels around the surface region reflects the long-range nature of the associated transition density between the 2_2^+ and 0_2^+ states, shown in Fig. 8a, and is responsible for the huge magnitude of DPP of the 0_2^++0_2^+ channel seen in Fig. 4. Namely, the dominant contribution of the 0_2^++2_2^+ and 2_2^++2_2^+ channels on DPP of the 0_2^++0_2^+ channel is originated from the spatially-extended 3α-cluster structure which is common to the 0_2^+ and 2_2^+ states. On the other hand, the negligible contribution to DPP of the 0_2^++0_2^+ channel from other channels, such as the 0_1^++2_1^+ and 2_1^++2_1^+ ones, is the consequence of the weak transition between the states having very different nuclear structures. Similarly, we can understand the reason why the dominant contribution to DPP in the elastic channel comes from the channels in which both ^{12}C nuclei are in the shell-like states, such as the 0_1^++2_1^+ and 2_1^++2_1^+ ones, and the reason why the contribution from other channels in which one or both ^{12}C nuclei are in the cluster-like states is negligible.

3.4 DPP for other partial waves and molecular bands

Now, we come back to the original folding-model potentials without DPP and investigate the molecular rotational bands composed of the barrier-top resonances generated by these folding-model potentials in the elastic channel as well as in the 0_2^++0_2^+ one. Figures 9a and 9b shows the partial cross sections for the "elastic scattering" by the real folding potential in the elastic (0_1^++0_1^+) channel and the 0_2^++0_2^+ one, respectively, for several partial waves, J(=L)=10, 12, 14, 16, 18 and 20. A sequence of sharp resonances are generated around the barrier top energy of each partial wave in the elastic channel, which form a molecular band with N=2n+L=18 and, hence, terminate at J=18. A sign of the appearance of N=20 band is also seen at several MeV above the N = 18 band but it is unclear because it lies well above the barrier-top energies and the resonance states have large widths. In the 0_2^++0_2^+ channel, there also observed are the series of sharp resonances slightly below the barrier-top energies, which

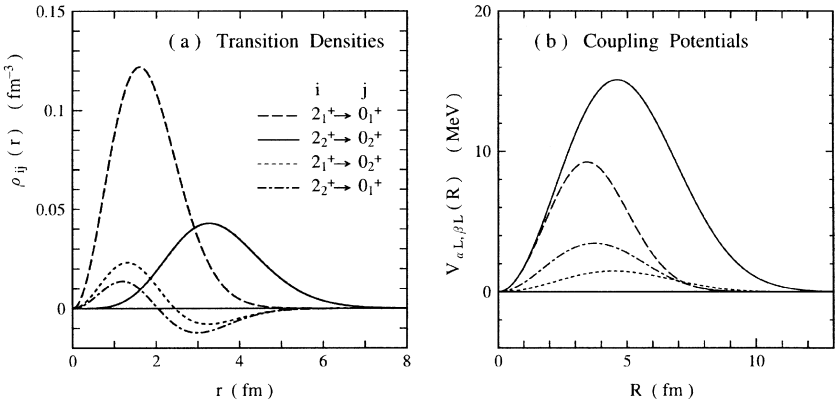

Fig. 8. (a) The quadrupole transition densities between the ^{12}C states indicated and (b) the coupling potentials associated to the transition density shown in (a). See text for the detai

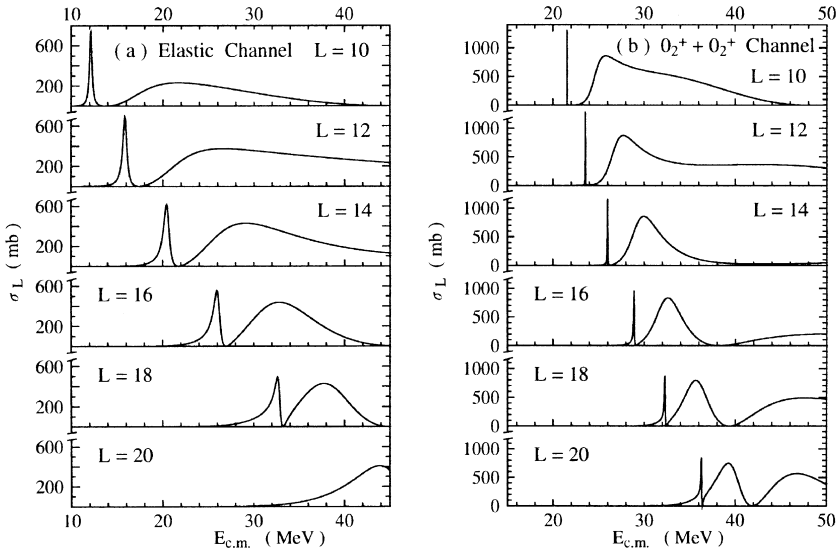

Fig. 9. The energy dependence of the partial cross sections for L=10∼20 of the single-channel potential scattering (a) in the elastic channel and (b) in the 0_2^++0_2^+ channel, where the folding-model potentials of the individual channels are used

are found to form a molecular band with N=2n+L=20 and hence terminate at J=20. In this channel, the N=22 band is also identified at about 4 MeV above the N=20 band with moderate widths. In this channel, there should also exist the N=18 band below the N=20 band for $J \leq$18 but it is not visible in the scattering due to the extremely small width. The resonance energies of these three bands are plotted in Fig. 10a by the open circles (for the elastic channel) and the open squares (for the 0_2^++0_2^+ channel) as a function of $J(J+1)$. It is noticed that the slope of the bands in the latter channel is smaller than that of the elastic band, which reflects the longer interaction range of the folding potential in the latter channel, as already mentioned before.

In the previous sections, we have seen for the J=18 partial wave that the channel coupling effect induces the strongly attractive DPP and that the addition of the attractive DPP to the original folding potential induces the new resonance state having the higher-nodal nature. We have performed the similar calculation for other partial waves (J=L=10, 12, 14 and 16) at the on-resonance energies of the above-mentioned potential resonances shown in Fig. 9 (those with N=18 for the elastic channel and with N=20 for the 0_2^++0_2^+ one) and we have confirmed the similar features of DPP as those we have seen at J=18. Namely, DPP is predominantly attractive around the nuclear surface and the effective potential modified with DPP for each partial wave generates the higher-nodal resonance state near the original resonance state generated by the folding potential. We have found that the wave function for each partial wave has n radial nodes inside the effective barrier with n satisfying N=2n+L=20 for the elastic channel and N=2n+L=28 for the 0_2^++0_2^+ one, as in the case of J=18. This implies that these newly generated resonance states may form a higher-nodal molecular-rotational band having a common oscillator quantum number N, provided they line up on straight lines in the $J(J+1)$ diagram.

To confirm this conjecture, we plot these new resonance states in the $J(J+1)$ diagram in Fig. 10a by the filled circles (for the elastic channel) and filled squares (for the 0_2^++0_2^+ one) connected by the solid lines, together with the original bands generated by the folding-model potential. As expected, the N=20 resonance states in the elastic channel line up very nicely on a straight line. Similarly, the N=28 resonance states in the 0_2^++0_2^+ channel almost line up on a line except for the J=16 state which largely deviates from the systematics of other partial waves. No addi-

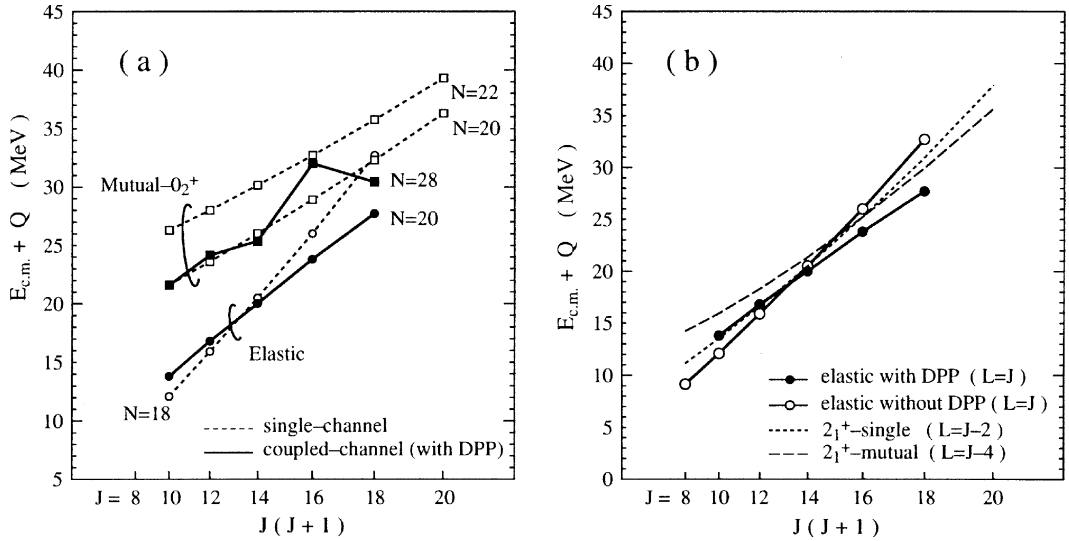

Fig. 10. (a) The rotational bands in the elastic channel and the 0_2^++0_2^+ one. The open circles (open squares) connected by the dotted lines indicate the single-channel resonances generated by the folding-model potential of the elastic channel (0_2^++0_2^+ channel), while the filled circles (filled squares) are the resonances generated by the folding-model potential supplemented by DPP in the respective channels. (b) The rotational bands in the elastic channel and the aligned (L=J-I) components of the rotational bands in the single-2_1^+ (dotted curve) and mutual-2_1^+ (dashed curve) channels. The elastic-channel bands are the same as those in (a). In the ordinate axis, Q denotes the Q-value of the excited channel

tional state with N=28 is found for J=16 around the expected energy of $E_{\rm c.m.}$ ≃29 MeV and, at present, the origin of the large deviation for the J=16 state is unknown. Hence, the formation of the N=28 "rotational band" in this channel is unclear but it is interesting to note that the energies of the J=16 and 18 resonance states in this channel lie in the energy range of the resonance observed in experiments ($E_{\rm c.m.}$ = 32.5 ± Γ/2 MeV with Γ ≃ 4 MeV). In fact, the CC calculation by Hirabayashi *et al.* [24], which reproduced this resonance, showed that the dominant partial waves were J=18 and 16 at the on-resonance energy $E_{\rm c.m.}$=32.5 MeV.

It is noticed that the new band in the elastic channel has a clearly smaller slope than the original band and these two bands cross each other between J=12 and 14. However, this does not implies that DPP is repulsive for the lower partial waves of J=10 and 12, because the new band consists of the higher-nodal states with N=20 while the original band has N=18. Therefore, DPP is still attractive for all the partial waves investigated here. The smaller slope implies that the moment of inertia of the new band becomes larger than that of the original band due to the increase of the barrier-top radius by the addition of the long-range attraction of DPP, which is already seen in Fig. 3.

It is also interesting to note that the slope of the new band in the elastic channel is close to the slope of the aligned band (L=J−2) in the 0_1^++2_1^+ channel and even closer to that of the aligned band in the 2_1^++2_1^+ channel with L=J−4, as shown by the dotted and dashed curves in Fig. 10b. The similarity of the slope may have a close relation to the fact that the dominant contribution to the elastic-channel DPP comes from these excited channels, although the aligned bands in these excited channels plotted here are the bands with N=18 same as the original elastic band (open circles), rather than N=20 of the newly-generated band (filled circles).

4 Summary and discussion

In this paper, we have investigated the effect of the channel coupling to the ^{12}C excited states in ^{12}C+^{12}C scattering in terms of the *dynamic polarization potential (DPP)* and its relation to the formation of molecular rotational bands in the elastic channel as well as in the 0_2^++0_2^+ one. This analysis has been made by the microscopic coupled-channel calculation with the use of the double-folding-model interactions based on the realistic nucleon-nucleon effective force and the reliable transition densities of ^{12}C obtained by the microscopic 3α-RGM calculation.

Because of the characteristic property of the ^{12}C nuclear structure, namely the coexistence of states having very different structure, the *shell-like states* and the *cluster-like states*, the elastic channel is mainly affected by the channels in which two ^{12}C nuclei are in the shell-like states, such as the 0_1^++2_1^+ and 2_1^++2_1^+ channels, while the 0_2^++0_2^+ channel is mainly affected by the channels in which two ^{12}C are in the cluster-like states, such as the 0_2^++2_2^+ and 2_2^++2_2^+ channels. These channel coupling effects are represented in terms of DPP for several grazing partial waves and it is found that DPP is attractive as a whole in the nuclear surface region in both the elastic channel and the 0_2^++0_2^+ one. In the elastic channel, the attractive DPP gives rise to about 5 MeV energy gain which generates the resonance state having an additional radial

node in its wave function compared with the original resonance state generated by the original potential without DPP added. The channel-coupling effect is particularly strong for the $0_2^+ + 0_2^+$ channel and DPP of this channel generated by the coupling to the $0_2^+ + 2_2^+$ and $2_2^+ + 2_2^+$ channels has an extremely strong attraction. This strong DPP gives rise to more than 20 MeV energy gain around the barrier region and generates the higher-nodal resonance state having four additional radial nodes compared with the resonance states generaged by the origial folding potential. The large effect of the channel coupling among the cluster-like channels is the consequence of the similarity of nuclear structure between the 0_2^+ and 2_2^+ states and the extended spatial range of the transition density between the states. These qualitative features of DPP are found to be almost independent of the incident energy and partial waves in the present molecular-resonance region.

Such a large correction term due to the channel coupling implies that the resonance state generated by the sum of the folding potential and DPP may not be a simple "potential resonance" to be observed only in the relevant channel for which we calculate DPP, but a more complex resonance state having partial decay widths to various exit channels. In other words, the resonance state is a kind of *eigenstate* having various components of the channels included in the CC calculation. Therefore, for example, it can be a case that some of the inelastic channels, such as the aligned component (L=$J-4$) of the $2_1^+ + 2_1^+$ channel, could be a dominant component of the resonance state (or eigenstate) and hence the elastic-channel component carries only a small fraction of the probability amplitude. In fact, it is found that this is the case of the present system. We have examined it by a test calculation in which the coupled-channels equations are solved by the variational calculation with the use of the L^2-integrable basis functions when all the imaginary potentials are switched-off, namely by the diagonalization of the matrix elements of the hermitian Hamiltonian of the present system, and examining the admixture of various channel components in the individual eigenstates. It is also found that the same is true for the *cluster-like eigenstates* generated by the coupling among the cluster-group of channels, where the "elastic" ($0_2^+ + 0_2^+$) component is found to have only a small probability amplitude. In the present paper, we do not discuss the details of this kind of analysis any further and a more complete analysis will be reported elsewhere in a forthcoming paper. We should, however, point out that the small elastic-channel component is represented in a different manner in the present study of DPP, namely, by the small amplitude of the wave function due to the imaginary part of DPP.

As we have already seen in Figs. 2 and 4, DPP has the absorptive imaginary part with a considerable strength in both the elastic channel and the $0_2^+ + 0_2^+$ one. The imaginary part of DPP represents the flux loss from the "entrance channel" (which corresponds to the elastic channel in the case of Fig. 2 and to the $0_2^+ + 0_2^+$ one in the case of Fig. 4) through the channel coupling and hence the amplitude of the wave function of that channel is strongly reduced compared with the case that only the real part of DPP is taken into account. In contrast to the imaginary potential $W(R)$ which was introduced in the diagonal potential (see (2.6)), the imaginary part of DPP does not necessarily represents the genuine absorption of flux to outside the model space of the CC calculation but it rather represents the flux flow from the entrance channel to various exit channels explicitly included in the CC calculation. Of course, DPP also contains the real absoption through the propagators of the inelastic channels, the denominator of which contains the distorting potential with the imaginary part $W(R)$. However, this is the higher-order effect of the imaginary potential in the intermediate channels. In fact, a very weak imaginary potential which we have adopted here for $W(R)$ will make this kind of higher-order effect small. Therefore, the imaginary part of DPP mainly represents the flux flow from the "entrance channel" to the "inelastic channels" within the CC model space. Thus, the suppressed amplitude of the entrance-channel wave function due to the imaginary part of DPP has a meaning similar to the small probability amplitude of the entrance-channel component observed in the variational approach. In any case, in order to understand the structure of the resonance states and its relation to the reaction dynamics, it is necessary to investigate the wave functions of all the relevant channels as well as the partial widths of the individual resonance states in more detail. This kind of analysis is in progress.

The strongly attractive effect of the channel coupling, represented by the real part of DPP, seems to lead to the formation of the new molecular-rotational bands which has the higher-nodal nature compared with the original molecular-rotational bands generated by the folding potential (although the formation of the rotational band is not so clear in the $0_2^+ + 0_2^+$ channel). Such a large correction to the real potential as well as the existence of the imaginary part of DPP with an appreciable strength suggest that these new type of rotational bands may consist of a series of resonance states (or *eigenstates*) having a considerable amount of the "inelastic-channel" components. Although in the present paper we have not yet confirmed the above conjecture, for example by the detailed anlysis of the resonance wave functions, the results of the present paper strongly suggest that the reaction dynamics leading to the resonance observed in experiments in the $0_2^+ + 0_2^+$ channel may not be so simple as to be understood by the simple band-crossing mechanism between the original (zeroth-order) molecular bands generated by the folding potential in each channel. It rather contains much more complicated dynamical processes through the strong coupling among the nearby channels having similar nuclear structure. On the other hand, we have also seen that the coupling between the different types of channels, the shell-like channels and the cluster-like ones, is weak and this fact allows us to expect that the transition between the above-mentioned new "rotational bands" (or "eigenbands") is also weak. This may suggest a new-type of band-crossing-like mechanism, which holds between the "eigenbands", each of which is generated by the strong

coupling among the same types of channels, rather than the "zeroth-order bands" generated by the folding-model potential. A more detailed analysis of this point, including the detailed analysis of the resonance wave functions and the partial widths, is in progress.

References

1. A.H. Wuosmaa, R.R. Betts, B.B. Back, M. Freer, B.G. Glagola, Th. Happ, D.J. Henderson, P. Wilt and I.G. Bearden, Phys. Rev. Lett. **68** (1992), 1295
2. A.H. Wuosmaa, M. Freer, B.B. Back, R.R. Betts, J.C. Gehring, B.G. Glagola, Th. Happ, D.J. Henderson, P. Wilt and I.G. Bearden, Phys. Rev. **C50** (1994), 2909
3. F. Ajzenberg-Selove, Nucl. Phys. **A506** (1990), 1
4. H. Morinaga, Phys. Rev. **101** (1956), 254; Phys. Lett. **21** (1966), 78
5. D.M. Brink, H. Freidrich, A. Weiguny and C. Wong, Phys. Lett. **33B** (1970), 143
6. N. Takigawa and A. Arima, Nucl. Phys. **A168** (1971), 593
7. Y. Suzuki, H. Horiuchi and K. Ikeda, Prog. Theor. Phys. **47** (1972), 1517
8. E. Uegaki, S. Okabe, Y. Abe and M. Tanaka, Prog. Theor. Phys. **57** (1977), 1262
9. M. Kamimura, Nucl. Phys. **A351** (1981), 456
10. G. Leander and S.E. Larsson, Nucl. Phys. **A239** (1975), 93
11. W. Bauhoff, H. Schultheis and R. Schultheis, Phys. Lett. **95B** (1980), 5; **106B** (1981), 278; Phys. Rev. **C22** (1980), 861; **C29** (1984), 1046
12. H. Flocard, P.H. Heenen, S.J. Kreiger and M.S. Weiss, Prog. Theor. Phys. **72** (1984), 1000
13. N. Cindro and W. Greiner, J. of Phys. **G9** (1983), L175
14. S. Marsh and W.D.M. Rae, Phys. Lett. **180B** (1986), 185
15. S.P.G. Chappell, D.L. Watson, S.P. Fox, C.D. Jones, W.D.M. Rae, P.M. Simmons, M. Freer, B.R. Fulton, N.M. Clarke, N. Curtis, M.J. Leddy, J.S. Pople, S.J. Hall, R.P. Ward, G. Tungate, W.N. Catfold, G.J. Gyapong, S.M. Singer and P.H. Regan, Phys. Rev. **C51** (1995), 695
16. R.M. Freeman, F. Haas, A. Elanique, A. Morsad and C. Beck, Phys. Rev. **C51** (1995), 3504
17. E.T. Mirgule, Suresh Kumar, M.A. Eswaran, D.R. Chakrabarty, V.M. Datar, N.L. Ragoowansi, H.H. Oza and U.K. Par, Nucl. Phys. **A583** (1995), 287
18. M. Aliotta, S. Cherubini, E. Costanzo, M. Lattuada, S. Romano, D. Vinciguerra and M. Zadro, Z. Phys. **A353** (1995), 43
19. M. Aliotta, S. Cherubini, E. Costanzo, M. Lattuada, S. Romano, C. Spitaleri, A. Tumino, D. Vinciguerra and M. Zadro, Z. Phys. **A354** (1996), 119
20. S. Szilner, Z. Basrak, R.M. Freeman, F. Haas, A. Morsad and C. Beck, Phys. Rev. **C55** (1997), 1312
21. R.A. Le Marechal, N.M. Clarke, M. Freer, B.R. Fulton, S.J. Hall, S.J. Hoad, G.R. Kelly, R.P. Ward, C.D. Jones, P. Lee and D.L. Watson, Phys. Rev. **C55** (1997), 1881
22. Y. Abe, *Nuclear Molecular Phenomina*, ed. N. Cindro (North Holland, Amsterdam, 1978); Y. Kondo, Y. Abe and T. Matsuse, Phys. Rev. **C19** (1979), 1356
23. Y. Abe, Y. Kondo and T. Matsuse, Prog. Theor. Phys. Suppl. No. 68 (1980), 303
24. Y. Hirabayashi, Y. Sakuragi and Y. Abe, Phys. Rev. Lett. **74** (1995), 4141
25. B.R. Fulton, T.M. Cormier and B.J. Herman, Phys. Rev. **C21** (1980), 198
26. S.F. Pate, R.W. Zurmühle, P.H. Kutt and A.H. Wuosmaa, Phys. Rev. **C37** (1988), 1953
27. Y. Sakuragi, *Heavy-Ion Reaction Dynamics in Tandem Energy Region*, eds. Y. Sugiyama, A. Iwamoto, H. Ikezoe (Universal Academy Press, Tokyo, 1989), p. 179
28. G.R. Satchler, *Direct Nuclear Reactions*, (Clarendon, Oxford, 1983), p.674; O. Tanimura and U. Mosel, Phys. Rev. **C24** (1981), 321
29. G.R. Satchler and W.G. Love, Phys. Rep. **55** (1979), 183
30. A.M. Kobos, B.A. Brown, R. Lindsay and G.R. Satchler, Nucl. Phys. **A384** (1982), 65; A.M. Kobos, B.A. Brown, P.E. Hodgson, G.R. Satchler and A. Budzanowski, Nucl. Phys. **A425** (1984), 205; M.E. Brandan and G.R. Satchler, Nucl. Phys. **A487** (1988), 477
31. M. El-Azab Farid and G.R. Satchler, Nucl. Phys. **A438** (1985), 525
32. G. Bertsch, J. Borysowicz, H. McManus and W.G. Love, Nucl. Phys. **A284** (1977), 399
33. Y. Sakuragi, M. Yahiro and M. Kamimura, Prog. Theor. Phys. **70** (1983), 1047
34. Y. Sakuragi, M. Yahiro and M. Kamimura, Prog. Theor. Phys. Suppl. No. 89 (1986), 136